Role of electron polarization in nuclear spin diffusion

Alessandro Chessari [1], Samuel F. Cousin [2], Sami Jannin [1], and Quentin Stern [1,*]
[1] *Univ Lyon, ENS Lyon, UCBL, CNRS, CRMN UMR 5082, F-69100, Villeurbanne, France*
[2] *Aix Marseille Université, CNRS, ICR, 13397 Marseille, France*

(Received 30 June 2022; revised 25 April 2023; accepted 7 June 2023; published 28 June 2023)

Dynamic nuclear polarization (DNP) is capable of boosting signals in nuclear magnetic resonance by orders of magnitude by creating out-of-equilibrium nuclear spin polarization. The diffusion of nuclear spin polarization in the vicinity of paramagnetic dopants is a crucial step for DNP and remains yet not well understood. In this paper, we show that the polarization of the electron spin largely controls the rate of proton spin diffusion in a DNP sample at 1.2 K and 7 T; at increasingly high electron polarization, spin diffusion vanishes. We rationalize our results using a 2 nucleus–1 electron model and Lindblad's master equation, which generalizes preexisting models in the literature and qualitatively accounts for the experimental observed spin diffusion dynamics.

DOI: 10.1103/PhysRevB.107.224429

I. INTRODUCTION

Dynamic nuclear polarization (DNP) [1–4] has enabled numerous applications in nuclear magnetic resonance (NMR) and magnetic resonance imaging (MRI), from real-time imaging of *in vivo* metabolism [5] to the study of active sites at the surface of catalysts [6], to list only two striking examples [7–9]. By creating an out-of-equilibrium nuclear polarization, DNP methods boost the sensitivity of magnetic resonance by sometimes up to 5 orders of magnitude [3], allowing for the detection of phenomena that are otherwise not observable. Solid-state DNP is amenable to many experimental conditions, whether performed on crystals [4,10] or frozen liquids [2], at low [11] or high magnetic field [12], and all the way down from 1 K [3] up to room temperature [13]. In all cases, it requires the presence of stable or transient unpaired electron spins [1,14]. The high polarization of the latter is transferred to the surrounding nuclei via microwave (μw) irradiation close to the resonance frequency of the electron spins. Nuclear spin diffusion then spreads out the polarization from those in the vicinity of the electron spin toward those further away in the bulk [15,16]. However, from the early days of DNP, it was recognized that the nuclei closest to the electron are unable to exchange polarization with their neighbors because their frequency is strongly shifted by the hyperfine interaction (HFI) with the electron. Indeed, the nuclear dipolar Hamiltonian is truncated by the HFI, which prevents energy-conservative nuclear flip-flops [17,18]. These magnetically isolated spins are often said to be within the so-called "spin diffusion barrier." 60 years after this concept has been introduced, it is still not clear at which distance from the electron nuclear spin diffusion starts being effective. Moreover, if diffusion is sometimes shown to be effective even where the dipolar interactions are presumably truncated, the mechanisms behind this phenomenon are not well understood yet [11,19–21].

We have recently introduced the hyperpolarization resurgence experiment (HypRes), a method that enables the observation of nuclear spin diffusion from nuclear spins nearby the electron, which are not accessible to direct NMR detection, to those further from the electron, which can be observed by NMR (the hidden and visible spins, respectively), as depicted in Fig. 1 [19]. Our measurements with the HypRes method revealed that proton spin diffusion had a strong temperature dependence between 1.2 and 4.2 K. Based on a mechanism proposed by Horvitz [22–27], we postulated that the electron polarization, which varies from 83% at 4.2 K to 99.93% at 1.2 K and 7.05 T, could be the key factor explaining the variation in nuclear spin diffusion in our observations.

In this paper, we confirm our hypothesis both experimentally and theoretically. Experimentally, we introduce an extension of the HypRes experiment where the electron polarization is lowered to a stable level by μw irradiation, which allows us to compare the efficiency of spin diffusion for various electron spin polarizations. We find that proton spin diffusion at 1.2 K in a glassy sample doped with TEMPOL is indeed faster when the electron polarization is reduced by μw irradiation. We then propose a new comprehensive model to estimate the efficiency of nuclear spin diffusion, accounting for the polarization of electron spins. Using theoretical tools common in quantum optics, we treat a pair of dipolar coupled nuclear spins as a two-level system in which transitions are driven by the quantum noise arising from the motion of a nearby electron spin. The influence of the nuclear spin bath on the two-level system is treated using Lindblad's master equation [28–32], which could be used to incorporate more complex relaxation mechanisms into the model. Previous models used perturbation theory to describe the drive provided by the electron spin noise but are only valid in the near vicinity of the electron spin [22–26]. Our model bridges the gap between this approach and spin diffusion mediated strictly by nuclear dipolar interactions [30,33–35] (which occurs only far from the electron in our case) and predicts a new coherent effect in the midrange.

*quentin.stern@protonmail.com

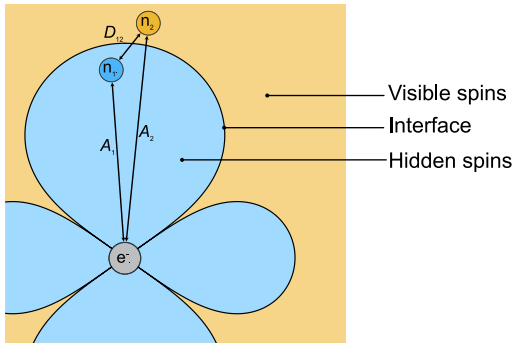

FIG. 1. Schematic representation of the hidden and visible nuclear spins interacting with the electron spin through the HFI with intensities A_1 and A_2. The two nuclei interact together with the dipole-dipole coupling constant D_{12}.

II. EXPERIMENTAL RESULTS

Figure 2(a) shows the pulse sequence of the HypRes experiment, similar to that in our previous work [19].

(i) The nuclear polarization is first wiped out by a series of saturation pulses.

(ii) The nuclear spins are polarized by μw irradiation until they reach DNP equilibrium during the delay t_{DNP}, setting the μw frequency so as to reach either positive or negative nuclear polarization.

(iii) The μw irradiation is gated and a delay t_g allows the electron spins to return to Boltzmann equilibrium [36,37].

(iv) The polarization of the visible spins is wiped out by a selective saturation scheme, optimized so as to saturate over a limited bandwidth of 200 kHz. The hidden spins are negligibly affected because the bandwidth of the saturation pulses is small compared to their hyperfine shifts.

(v) The equilibration of polarization between the visible and hidden spins is monitored using small-angle pulses.

We performed the μw-off HypRes experiment as in Ref. [19] on a sample of 50 mM TEMPOL in H_2O:D_2O:D_8-

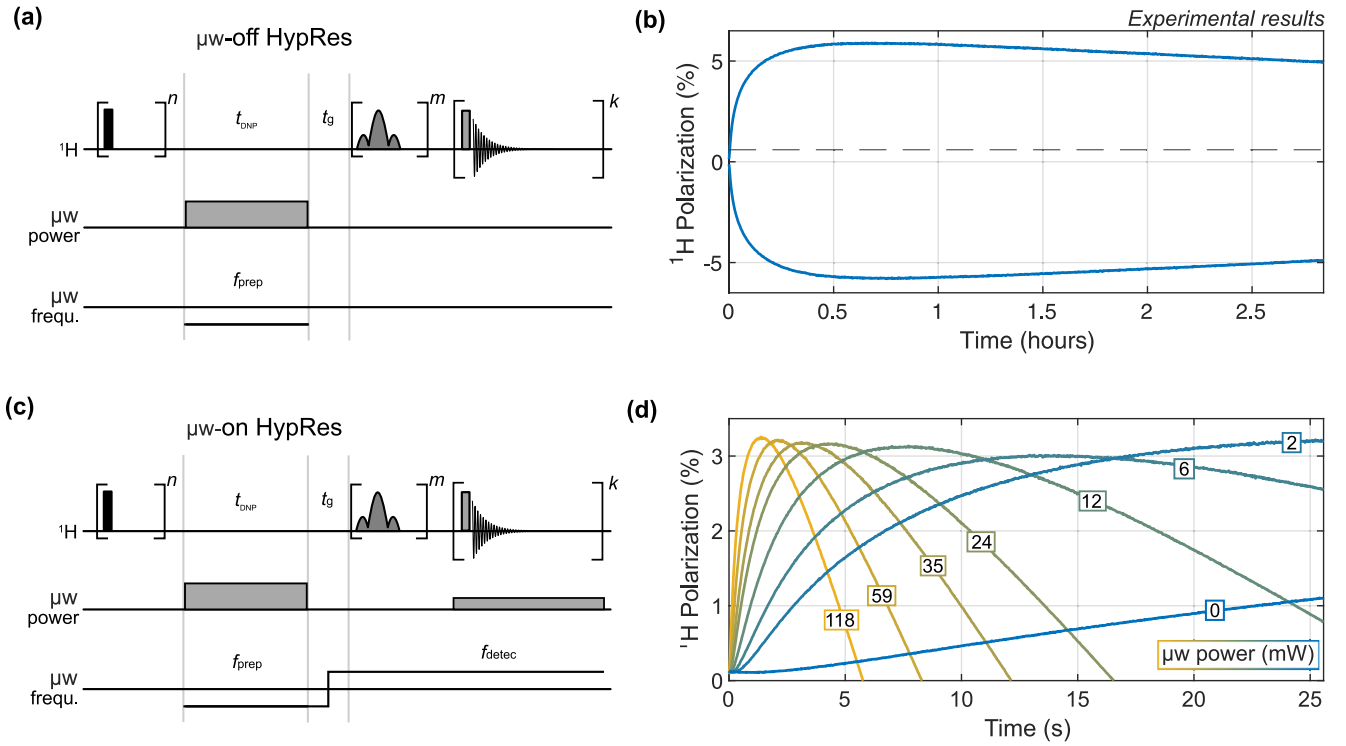

FIG. 2. Pulse sequence diagrams [panels (a) and (c), respectively] and results of the μw-off and -on HypRes experiments at 7.05 T and 1.2 K [panels (b) and (d), respectively]. On the ^{1}H channel of the pulse sequence diagram, the black and gray rectangles represent square pulses, with nutation angles of $\pi/2$ and 0.1 deg, respectively. After an initial strong saturation with $n = 120\ \pi/2$ deg pulses, μw irradiation was switched on at the maximum available power during delay $t_{DNP} = 640$ s of the preparation at a frequency f_{prep} of 197 648 and 198 112 MHz for positive and negative DNP, respectively, with a sawtooth frequency modulation of 160 MHz around the central frequency, at a rate of 500 Hz. After switching off μw irradiation, a delay $t_g \approx 10$ s let the electron relax toward Boltzmann equilibrium, before the detection was launched. The train of $m = 19$ sinc pulses separated by random delays saturated the visible spins (see the Supplemental Material [38] for more detail on the saturation scheme). Finally, the HypRes signal was recorded $k = 1024$ times, with 0.1 deg pulses every 10 s and 0.025 s in the case of the μw-off and -on experiments, respectively. The μw-off HypRes experiments on panel (b) were recorded with both positive and negative DNP during preparation, causing a positive and negative polarization overshoot, respectively. The horizontal dashed line on panel (b) indicates the Boltzmann equilibrium polarization of proton spins. In the case of the μw-on HypRes experiments, μw irradiation was switched back on after saturation at a specific power and frequency f_{detec}. The μw-on HypRes experiments were recorded with positive DNP during preparation and negative DNP during detection. The μw power applied during detection from 0 to 118 mW is indicated on the curves of panel (d).

glycerol 1:3:6 (v/v/v) (DNP juice) at 1.2 K and 7.05 T in a liquid helium bath cryostat [41]. The experiment was performed setting the μw frequency during preparation so as to reach either positive or negative nuclear polarization, with a polarization $P_{\mathrm{DNP}}^{\mathrm{max}}$ on the order of +70% and −70%, respectively (see the Supplemental Material [38] for more details on polarization quantification). The positive (or negative) polarization acquired during preparation was wiped out by the saturation pulses only for the visible spins, far from the electron (<0.2% remaining polarization). The spins closer to the electron retained their polarization, which is invisible by NMR (due to large hyperfine shifts); this polarization surged onto the visible spins during the course of detection, causing an observable positive overshoot (or negative, respectively). The two resulting curves are shown in Fig. 2(b). The Boltzmann equilibrium polarization of proton spins is indicated by a dashed line for comparison (0.60% in these conditions). The experimental traces feature two processes: the equilibration of the hidden and visible spins polarizations via spin diffusion far beyond Boltzmann equilibrium within ≈0.5 h, followed by their slow relaxation toward it. The spin diffusion process monitored during the first part occurs while the electron polarization is that of Boltzmann equilibrium, which is 99.93% in these conditions.

In order to monitor spin diffusion in the same conditions but with a lower electron polarization, we repeated the experiment using the pulse sequence presented in Fig. 2(c). In this case, after μw irradiation was switched off, the μw frequency was changed from the value yielding positive nuclear spin polarization to that yielding negative polarization. μw irradiation was then switched back on during detection. This experiment was repeated with different values of μw power during detection from 0 to 118 mW, yielding the curves shown on Fig. 2(d). The μw power used during detection is indicated on the curves. Like for the μw-off HypRes experiment, the nuclear polarization acquired by the hidden spins during preparation first surged onto the visible spins causing a positive polarization overshoot. Then, instead of decaying toward thermal equilibrium (only 0.60% polarization), negative DNP started pulling the polarization toward the opposite direction at the negative DNP equilibrium value. Most importantly, the stronger the μw power during the equilibration of polarization between the visible and hidden spins, the weaker the electron polarization, and hence the faster the flow of nuclear polarization from the hidden to the visible spins. μw irradiation does not influence the nuclei other than through the electron spins (the sample space heating by μw irradiation is less than 10 mK). Therefore, only the electron dynamics can be responsible for the observed rapid spin diffusion from hidden to visible spins.

III. THEORY

To understand how electron spin polarization influences nuclear spin diffusion, we calculate the transition rate probability W between the states $|\alpha\beta\rangle$ and $|\beta\alpha\rangle$ of a pair of coupled nuclei, at an internuclear distance a, with dipolar coupling constant D_{12}, both subject to the dipolar field of an electron spin, at distances r_i and with hyperfine coupling constants $A_{z,i}$, as shown in Fig. 1. Following Horvitz's idea [22] the electron is treated semiclassically, taking into account the stochastic time dependence of its state. Because of the high radical concentration of 50 mM, electron spins are strongly dipolar coupled, and the correlation time of their spin state τ_c is dominated by their dipolar couplings, in contrast with Horvitz's case, where τ_c was dominated by the electron spin-lattice relaxation. Note that μw irradiation only affects a small subset of electron spins directly. However, due to fast spectral diffusion, the whole electron spin bath is indirectly affected by μw irradiation. Finally, we note that the energy associated with the transfer of nuclear Zeeman energy throughout the sample is small compared with that of the electron dipolar energy, which allows us to treat electron dynamics as unaffected by nuclear dynamics.

To calculate the nuclear flip-flop transition rate probability we can restrict the Hilbert space to the $|\alpha\beta\rangle$ and $|\beta\alpha\rangle$ subspace. The restricted nuclear dipolar and hyperfine Hamiltonians are expressed in terms of the Pauli matrices $\hat{\sigma}_{\pm} = \hat{I}_1^{\pm}\hat{I}_2^{\mp}$ and $\hat{\sigma}_z = 2(\hat{I}_1^z - \hat{I}_2^z)$ as follows,

$$\hat{H}_D = -\tfrac{1}{2}D_{12}(\hat{\sigma}_+ + \hat{\sigma}_-), \tag{1}$$

$$\hat{H}_{HF}(t) = \tfrac{1}{2}\Delta[\bar{P} + P'(t)]\hat{\sigma}_z, \tag{2}$$

respectively, where $\Delta = A_{z,1} - A_{z,2}$ is the difference of the HFI. For simplicity, we ignore any diagonal terms giving rise to an overall shift of the two energy levels. The dynamics of the electron polarization $P(t)$ is decomposed into a static contribution given by the average value $\bar{P}$ and an unbiased signal $P'(t)$, with an autocorrelation function $R(\tau) = (1-\bar{P}^2)e^{-\Gamma_c|\tau|}$, where $\tau_c = 1/\Gamma_c$ is the correlation time of the electron spin state [22,42], as detailed in the Supplemental Material [38]. In the rotating frame given by $U_0 = e^{-i\int_0^t \hat{H}'_{HF}(\tau)d\tau}$, the Hamiltonian reads

$$\hat{H} = \tfrac{1}{2}\Delta\bar{P}\hat{\sigma}_z - \tfrac{1}{2}D_{12}[\hat{\sigma}_+ f(t) + \hat{\sigma}_- f^*(t)], \tag{3}$$

and describes a two-level system excited by the drive $f(t) = e^{i\Delta\int_0^t P'(s)ds}$. Since the electron dynamics is stochastic, the spectrum of $f(t)$ is calculated averaging over all the possible $P'(t)$ processes yielding [43–45]

$$F(\omega) = \frac{2\Gamma_c(1-\bar{P}^2)\Delta^2}{[\omega^2 - (1-\bar{P}^2)\Delta^2]^2 + \omega^2\Gamma_c^2}, \tag{4}$$

which is similar to what Horvitz obtained using a perturbative approach. The excitation spectrum is calculated from the correlator $\langle\hat{\sigma}_-(\tau)\hat{\sigma}_+(0)\rangle$ where the presence of the nuclear spin bath and the pseudosecular hyperfine interaction are treated using the relaxation superoperator in Lindblad's form (with $\mathcal{D}(\hat{X})\cdot = X^\dagger\cdot X - \frac{1}{2}\{X^\dagger X, \cdot\}$; see the Supplemental Material [38]),

$$\mathbf{\Gamma} = \sum_{i=1,2}\Gamma_{1,i}[\mathcal{D}(\hat{I}_{i+}) + \mathcal{D}(\hat{I}_{i-})] + \frac{\Gamma_2^{(II)}}{2}\mathcal{D}(\hat{\sigma}_z). \tag{5}$$

The nuclear spin-lattice relaxation is dominated by the pseudosecular hyperfine interaction $A_{\pm,i}$,

$$\Gamma_{1,i} = \tfrac{1}{2}A_{+,i}A_{-,i}(1-\bar{P}^2)\frac{\Gamma_c}{\Gamma_c^2 + \omega_0^2}, \tag{6}$$

where ω_0 is the nuclear Larmor frequency, while the nuclear zero-quantum relaxation rate (the decay rate of the coherences

in the $|\alpha\beta\rangle$, $|\beta\alpha\rangle$ subsystem) is dominated by the interaction of nuclear spins i with their neighbors k through the couplings D_{ik} [33],

$$\Gamma_2^{(II)} \approx \sum_{k\neq 1,2} (D_{1k} - D_{2k})^2 \tau_{c,n}, \tag{7}$$

where $\tau_{c,n}$ is the nuclear correlation time.

The excitation spectrum has a Lorentzian shape centered at the energy difference $\Delta\bar{P}$,

$$S_{\Gamma_2}(\omega - \Delta\bar{P}) = \frac{2\Gamma_2}{(\omega + \Delta\bar{P})^2 + \Gamma_2^2}, \tag{8}$$

where we have introduced the effective broadening of the levels due to the environment $\Gamma_2 = \sum_{i=1,2} \Gamma_{1,i} + \Gamma_2^{(II)}$. The transition rate probability of the nuclear flip-flop is given by the integral [43,46,47]

$$\begin{aligned} W &= \frac{D_{12}^2}{4}\frac{1}{2\pi}\int_{-\infty}^{\infty} S_{\Gamma_2}(\omega' - \Delta\bar{P})F(\omega')d\omega' \\ &= \frac{D_{12}^2}{2}\frac{\Gamma_c(1-\bar{P}^2)\Delta^2 + \Gamma_2(\bar{\Gamma}^2 + \Delta^2)}{[(1-2\bar{P}^2)\Delta^2 + \Gamma_2\bar{\Gamma}]^2 + \Delta^2\bar{P}^2(\Gamma_2 + \bar{\Gamma})^2}, \end{aligned} \tag{9}$$

where $\bar{\Gamma} = \Gamma_c + \Gamma_2$. The expression of the transition rate depends explicitly on electron polarization. In the limit $\bar{P} \to 1$, Eq. (10) is equal to the transition rate between two nondegenerate nuclear levels commonly found in the literature [30,33–35,48].

In the limit of long τ_c, the nuclear flip-flop rate simplifies to an expression that can be expressed as the sum of two contributions $W_{(+)}$ and $W_{(-)}$ with

$$W_{(\pm)} = \frac{D_{12}^2}{4}\frac{\Gamma_2 + \Gamma_c/2}{(\Delta\bar{P} \pm \Delta\sqrt{1-\bar{P}})^2 + (\Gamma_2 + \Gamma_c/2)^2}. \tag{10}$$

In the opposite case of short τ_c, the electron spin fluctuations become too fast to drive transitions and only contribute to spin diffusion by broadening the nuclear levels, yielding

$$W = \frac{D_{12}^2}{2}\frac{\Gamma_{2*}}{\Delta^2\bar{P}^2 + \Gamma_{2*}^2}, \tag{11}$$

with $\Gamma_{2*} = \Gamma_2 + \frac{1}{\Gamma_c}(1-\bar{P}^2)\Delta^2$.

Based on the transition rate, the nuclear spin diffusion coefficient is calculated as $D = Wa^2$, with a the average internuclear distance, following Bloembergen [15,49]. Figure 3(a) shows the diffusion coefficient as a function of the distance of the closest nucleus to the electron for various electron polarizations. The dipolar interaction D_{12} and the HFI $A_{z,1}$ and $A_{z,2}$ were averaged over all orientations so that the diffusion coefficient depends only on r (and not on the angles between the vectors connecting the spins and the magnetic field). The nuclear coherence decay rate was approximated from the experimental FWHM $\delta\nu_{1/2}$, as $\Gamma_2^{(II)} \approx \delta\nu_{1/2}/2 \approx 11$ kHz (see the Supplemental Material [38] for the measurement of the $\delta\nu_{1/2}$). The grayed area represents the distance to the electron where the assumption that the nuclear spins experience an average value of the HFI is no longer valid, i.e., $\Gamma_c < |A_{i,j}|$. The black and gray vertical lines indicate the radius of mean volume per electron r_{MV} and the radius of the hidden spin reservoir $r_h = 0.9$ nm, respectively (which we define as the interface between the hidden and visible spins, where the proton spins have a coupling of 100 kHz with the electron). As depicted by the hollow circles in Fig. 3, our model predicts that spin diffusion at the interface between the visible and hidden spins is ≈17 times faster when the electron polarization is $\bar{P} \approx 50\%$ (that is, under μw irradiation [36,37]) compared to that at Boltzmann equilibrium $\bar{P} = 99.93\%$. The contrast of spin diffusion between μw-on and -off is even stronger closer to the electron.

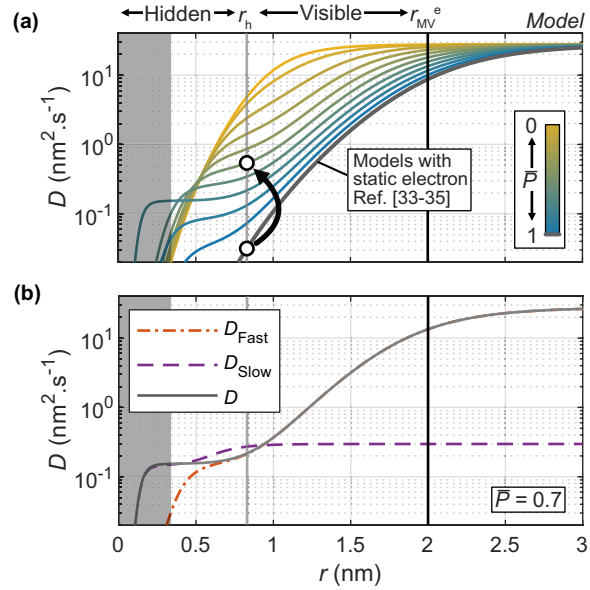

FIG. 3. (a) Calculated spin diffusion coefficient as a function of the distance to the electron for the same spin system for different electron polarization $\bar{P}$ between 0 and 1 in steps of 0.1 [see Eq. (9)]. The vertical black and gray lines represent the radius of the mean volume per electron and the limit between the visible and hidden spins, respectively. The gray area indicates the region where the model hypothesis breaks down ($\Gamma_c < |A_{i,j}|$; see text). The arrow between the two hollow circles indicates the increase in diffusion coefficient upon switching on μw irradiation. (b) Calculated spin diffusion coefficient in the fast and slow motion approximations [see Eqs. (11) and (10), respectively] compared with the exact solutions [see Eq. (9)], for $\bar{P} = 0.7$. The nuclear interdistance a, the nuclear broadening due to nucleus-nucleus interactions, and the electron correlation time $1/\Gamma_c$ are assumed to be 0.66 nm, 11 kHz, and 0.5 μs, respectively.

Although the single electron of our model has a unique value of τ_c, this value can be in the long or short limit [see Eqs. (10) and (11), respectively], depending on distance r. Figure 3(b) shows the diffusion coefficient computed based on the exact transition rate [see Eq. (9)] or on the approximated rates for long and short τ_c [see Eqs. (10) and (11), respectively], for $\bar{P} = 0.7$. Close to the electron, the separation $\Delta\bar{P}$ between the nuclear levels is large and the electron spin fluctuations are slow in comparison. Far from the electron, the nuclear levels are closer and the electron spin fluctuations are fast in comparison. As a consequence, the diffusion coefficients computed using the transition probability under the slow and fast limit coincide with the exact expression close and far from the electron, respectively.

IV. DISCUSSION

The rate at which polarization rises in the HypRes curves (see Fig. 2) is sensitive to the spin diffusion coefficient at the interface between the hidden and visible spins. As we have seen, when the polarization of the electron approaches unity, diffusion is dramatically reduced. In that sense, our theoretical model matches qualitatively with our experimental observations. Because DNP occurs under μw irradiation, that is, at low electron polarization, both our experimental results and our theoretical model lead to the conclusion that spin diffusion in the vicinity of the electron is efficient in our conditions, precisely when DNP is active. Because the mechanism for spin diffusion relies on fluctuations of the electron spin state, it should be sensitive to the radical concentration; at lower radical concentrations, electron-electron interactions would be weaker and τ_c longer, resulting in weaker nuclear spin diffusion [50]. In the limit of noninteracting electron spins, this spin diffusion mechanism should still be active but τ_c would be dominated either by electron spin-lattice relaxation or by μw irradiation, the latter case corresponding to hyperfine decoupling [21].

Our model is based on simplifying assumptions which could be improved in several ways. First, we have assumed that the decorrelation rate of the electron spin state Γ_c is large compared to the HFI but this assumption breaks down at $r = 0.34$ nm (see Fig. 3). A more precise calculation would require the use of slow-motion theories [51]. Moreover, we have only considered the anisotropic part of the HFI. Improving these points would be necessary if one intends to treat the important case of nuclei on the radical molecule. We have only considered 2-spin order but considering coupled spin terms between more than two spins could lead to predicting faster spin diffusion [35]. We have represented the electron spin state using a spectral density function assuming a homogeneous positive electron polarization. Yet, the predicted number of flip-flops could be higher if the non-Zeeman spin temperature of the electron is considered as it leads to significant variation of electron spin polarization along the spectrum of the electron spin, even though with an apparent constant average Zeemann polarization. We found that, in this sample, spin diffusion in the vicinity of the electron is effectively quenched when the electron polarization approaches unity. In other samples, other mechanisms that couple the nuclear spins to the lattice phonons could be at play [52]. In particular, methyl rotation which is still active at temperatures as low as 1 K could contribute to enhancing spin diffusion [53].

V. CONCLUSION

We showed both experimentally and theoretically that the rate of proton spin diffusion at 1.2 K and 7.05 T depends on the level of electron polarization: the lower the electron polarization, the faster spin diffusion. To do so, we introduced an extension of the HypRes experiment [19] to monitor nuclear spin diffusion in the vicinity of the electron spin while controlling the level of electron polarization via μw irradiation. We have constructed a model to understand the influence of electron polarization on nuclear spin diffusion. When the electron correlation time is comparable to the timescale of the nuclear flip-flops, a coherent mechanism enhances nuclear spin diffusion. Our model gives a recipe to estimate the diffusion efficiency as a function of the average polarization and correlation time of the electron spin. When electron polarization is slightly below unity and in the proximity of the electron, it is equivalent to that of Horvitz [22].

DNP was simulated in large spin systems including nuclear spin diffusion in a number of studies, where electron flip-flops were not included as a drive for nuclear spin diffusion [30,35,48,54–56]. Our results show the dramatic influence of this mechanism on spin diffusion. Other mechanisms of electron-driven nuclear spin diffusion have been reported in the context of MAS-DNP [57–59] and ^{13}C hyperpolarization with color centers in diamonds [60,61]. The mechanism that we have highlighted in this work could potentially be at play in such contexts and therefore contribute to a better understanding of spin diffusion in dDNP as well as in other types of DNP experiments [11,20,21,62]. From the understanding offered by our results, new sample architectures could be devised to optimize spin diffusion in the context of hyperpolarized NMR. On the contrary, the same design principles could be used to minimize spin diffusion and prevent losses of quantum information in spin qubit systems [63,64].

ACKNOWLEDGMENTS

We thank C. Bengs for his comments on the manuscript and for insightful discussions on Lindblad's master equation. We thank F. Mentink-Vigier and A. Pell for enlightening discussions. We acknowledge Bruker Biospin for providing the prototype dDNP polarizer and particularly D. Eshchenko, R. Melzi, M. Rossire, M. Sacher, and J. Kempf for scientific and technical support. We additionally acknowledge C. Jose and C. Pages for use of the ISA Prototype Service, and S. Martinez of the UCBL mechanical workshop for machining parts of the experimental apparatus. This research was supported by ENS-Lyon, the French CNRS, Lyon 1 University, the European Research Council under the European Union's Horizon 2020 research and innovation program (ERC Grant Agreement No. 714519/HP4all and Marie Skłodowska-Curie Grant Agreement No. 766402/ZULF), and the French National Research Agency (Project HyMag No. ANR-18-CE09-0013).

[1] A. W. Overhauser, Phys. Rev. **92**, 411 (1953).
[2] D. A. Hall, D. C. Maus, G. J. Gerfen, S. J. Inati, L. R. Becerra, F. W. Dahlquist, and R. G. Griffin, Science **276**, 930 (1997).
[3] J. H. Ardenkjær-Larsen, B. Fridlund, A. Gram, G. Hansson, L. Hansson, M. H. Lerche, R. Servin, M. Thaning, and K. Golman, Proc. Natl. Acad. Sci. USA **100**, 10158 (2003).
[4] M. Duijvestijn, C. Van Der Lugt, J. Smidt, R. Wind, K. Zilm, and D. Staplin, Chem. Phys. Lett. **102**, 25 (1983).
[5] K. Golman, R. in 't Zandt, and M. Thaning, Proc. Natl. Acad. Sci. USA **103**, 11270 (2006).
[6] T. Kobayashi, F. A. Perras, I. I. Slowing, A. D. Sadow, and M. Pruski, ACS Catal. **5**, 7055 (2015).

[7] B. Plainchont, P. Berruyer, J.-N. Dumez, S. Jannin, and P. Giraudeau, Anal. Chem. **90**, 3639 (2018).

[8] S. Jannin, J.-N. Dumez, P. Giraudeau, and D. Kurzbach, J. Magn. Reson. **305**, 41 (2019).

[9] Z. J. Wang, M. A. Ohliger, P. E. Larson, J. W. Gordon, R. A. Bok, J. Slater, J. E. Villanueva-Meyer, C. P. Hess, J. Kurhanewicz, and D. B. Vigneron, Radiology **291**, 273 (2019).

[10] C. Jeffries, Proc. R. Soc. London A **283**, 471 (1965).

[11] K. O. Tan, M. Mardini, C. Yang, J. H. Ardenkjær-Larsen, and R. G. Griffin, Sci. Adv. **5**, eaax2743 (2019).

[12] M. Rosay, M. Blank, and F. Engelke, J. Magn. Reson. **264**, 88 (2016).

[13] S. Fujiwara, N. Matsumoto, K. Nishimura, N. Kimizuka, K. Tateishi, T. Uesaka, and N. Yanai, Angew. Chem., Int. Ed. **61**, e202115792 (2022).

[14] V. Michaelis, R. Griffin, B. Corzilius, and S. Vega, *Handbook of High Field Dynamic Nuclear Polarization* (John Wiley & Sons, 2020).

[15] N. Bloembergen, Physica **15**, 386 (1949).

[16] G. R. Khutsishvili, Sov. Phys. Usp. **8**, 743 (1966).

[17] W. Blumberg, Phys. Rev. **119**, 79 (1960).

[18] G. R. Khutsishvili, Sov. Phys. JETP **15**, 909 (1962).

[19] Q. Stern, S. F. Cousin, F. Mentink-Vigier, A. C. Pinon, S. J. Elliott, O. Cala, and S. Jannin, Sci. Adv. **7**, eabf5735 (2021).

[20] S. K. Jain, C.-J. Yu, C. B. Wilson, T. Tabassum, D. E. Freedman, and S. Han, Chem **7**, 421 (2021).

[21] N. Wili, J. H. Ardenkjær-Larsen, and G. Jeschke, Magn. Reson. Discuss. **2022**, 1 (2022).

[22] E. P. Horvitz, Phys. Rev. B **3**, 2868 (1971).

[23] J. Wolfe, Phys. Rev. Lett. **31**, 907 (1973).

[24] L. L. Buishvili, M. D. Zviadadze, and B. D. Mikaberidze, Zh. Eksp. Teor. Fiz **69**, 2118 (1975).

[25] K. K. Sabirov, Phys. Status Solidi B **91**, 735 (1979).

[26] V. A. Atsarkin and V. V. Demidov, Zh. Eksp. Teor. Fiz **79**, 1438 (1980).

[27] C. Ramanathan, Appl. Magn. Reson. **34**, 409 (2008).

[28] G. Lindblad, Commun. Math. Phys. **48**, 119 (1976).

[29] V. Gorini, A. Kossakowski, and E. C. G. Sudarshan, J. Math. Phys. **17**, 821 (1976).

[30] A. Karabanov, G. Kwiatkowski, and W. Köckenberger, Mol. Phys. **112**, 1838 (2014).

[31] C. Bengs and M. H. Levitt, J. Magn. Reson. **310**, 106645 (2020).

[32] A. J. Pell, J. Magn. Reson. **326**, 106939 (2021).

[33] D. Suter and R. R. Ernst, Phys. Rev. B **32**, 5608 (1985).

[34] M. Ernst and B. H. Meier, Stud. Phys. Theor. Chem. **84**, 83 (1998).

[35] A. Karabanov, D. Wiśniewski, F. Raimondi, I. Lesanovsky, and W. Köckenberger, Phys. Rev. A **97**, 031404(R) (2018).

[36] A. Bornet, A. Pinon, A. Jhajharia, M. Baudin, X. Ji, L. Emsley, G. Bodenhausen, J. H. Ardenkjaer-Larsen, and S. Jannin, Phys. Chem. Chem. Phys. **18**, 30530 (2016).

[37] D. Guarin, D. Carnevale, M. Baudin, P. Pelupessy, D. Abergel, and G. Bodenhausen, J. Phys. Chem. Lett. **13**, 175 (2022).

[38] See Supplemental Material at http://link.aps.org/supplemental/10.1103/PhysRevB.107.224429 for the polarization quantification of the data in Fig. 2, the experimental and theoretical determination of the saturation width for the experiments in Fig. 2, the experimental estimation of the nuclear broadening used to compute the model, and the derivation of the model. The Supplemental Material also contains Refs. [39,40].

[39] A. J. Pell, G. Pintacuda, and C. P. Grey, Prog. Nucl. Magn. Reson. Spectrosc. **111**, 1 (2019).

[40] D. Manzano, AIP Adv. **10**, 025106 (2020).

[41] S. J. Elliott, Q. Stern, M. Ceillier, T. El Daraï, S. F. Cousin, O. Cala, and S. Jannin, Prog. Nucl. Magn. Reson. Spectrosc. **126-127**, 59 (2021).

[42] R. Fitzhugh, Math. Biosci. **64**, 75 (1983).

[43] J. Li, M. P. Silveri, K. S. Kumar, J.-M. Pirkkalainen, A. Vepsäläinen, W. C. Chien, J. Tuorila, M. A. Sillanpää, P. J. Hakonen, E. V. Thuneberg, and G. S. Paraoanu, Nat. Commun. **4**, 1420 (2013).

[44] D. Walls and G. Milburn, *Quantom Optics* (Springer, 1994).

[45] C. W. Gardiner and P. Zoller, *Quantum Noise: A Handbook of Markovian and Non-Markovian Quantum Stochastic Methods with Applications to Quantum Optics* (Springer, 2004).

[46] M. P. Silveri, J. A. Tuorila, E. V. Thuneberg, and G. S. Paraoanu, Rep. Prog. Phys. **80**, 056002 (2017).

[47] K. Wódkiewicz, B. W. Shore, and J. H. Eberly, Phys. Rev. A **30**, 2390 (1984).

[48] A. Karabanov, D. Wiśniewski, I. Lesanovsky, and W. Köckenberger, Phys. Rev. Lett. **115**, 020404 (2015).

[49] I. J. Lowe and S. Gade, Phys. Rev. **156**, 817 (1967).

[50] B. A. Rodin, V. Thalakottoor, M. Baudin, N. Birilirakis, G. Bodenhausen, A. V. Yurkovskaya, and D. Abergel, Phys. Chem. Chem. Phys. **25**, 15040 (2023).

[51] N. Benetis, J. Kowalewski, L. Nordenskiöld, H. Wennerström, and P.-O. Westlund, Mol. Phys. **48**, 329 (1983).

[52] J. Dolinšek, P. Cereghetti, and R. Kind, J. Magn. Reson. **146**, 335 (2000).

[53] B. Meier, J.-N. Dumez, G. Stevanato, J. T. Hill-Cousins, S. S. Roy, P. Håkansson, S. Mamone, R. C. Brown, G. Pileio, and M. H. Levitt, J. Am. Chem. Soc. **135**, 18746 (2013).

[54] Y. Hovav, A. Feintuch, and S. Vega, J. Magn. Reson. **207**, 176 (2010).

[55] Y. Hovav, A. Feintuch, and S. Vega, J. Magn. Reson. **214**, 29 (2012).

[56] D. Shimon, Y. Hovav, A. Feintuch, D. Goldfarb, and S. Vega, Phys. Chem. Chem. Phys. **14**, 5729 (2012).

[57] J. J. Wittmann, M. Eckardt, W. Harneit, and B. Corzilius, Phys. Chem. Chem. Phys. **20**, 11418 (2018).

[58] F. Mentink-Vigier, S. Vega, and G. De Paëpe, Phys. Chem. Chem. Phys. **19**, 3506 (2017).

[59] F. A. Perras and M. Pruski, J. Chem. Phys. **151**, 034110 (2019).

[60] D. Pagliero, P. R. Zangara, J. Henshaw, A. Ajoy, R. H. Acosta, J. A. Reimer, A. Pines, and C. A. Meriles, Sci. Adv. **6**, eaaz6986 (2020).

[61] D. Pagliero, P. R. Zangara, J. Henshaw, A. Ajoy, R. H. Acosta, N. Manson, J. A. Reimer, A. Pines, and C. A. Meriles, Phys. Rev. B **103**, 064310 (2021).

[62] N. A. Prisco, A. C. Pinon, L. Emsley, and B. F. Chmelka, Phys. Chem. Chem. Phys. **23**, 1006 (2021).

[63] J. Chen, C. Hu, J. F. Stanton, S. Hill, H.-P. Cheng, and X.-G. Zhang, J. Phys. Chem. Lett. **11**, 2074 (2020).

[64] D. D. Awschalom, R. Hanson, J. Wrachtrup, and B. B. Zhou, Nat. Photonics **12**, 516 (2018).